Journal of Applied Sciences and Emerging Technologies Vol. 1, Issue 1, 2023

A Modified Battery Charger with Power Factor Correction for Plug-in Electrical Vehicles

Arfa Tariq [1]*

* [1]Department of Electrical Engineering, COMSATS University Lahore, Islamabad Campus, Pakistan
arfatariq@cuilahore.edu.pk

Abstract: Electrical vehicles are becoming famous worldwide having the striking benefits of improved energy efficiency and reduced carbon footprints etc. Plug-in Electrical Vehicles (PEVs) are powered by batteries and these batteries needs to be recharged after every usage cycle. These batteries are fully charged at terminal voltage of 420 V and the voltage drops to 300 V after the usage cycle. Therefore, these batteries would require a battery charger ranging from 300V-420V to fully charge the batteries. There are two type of on-board battery chargers, 1) Two-stage and single-stage chargers. The former has drawbacks of larger component count, larger size and lower efficiency. Hence, in this research project, a single-stage battery charger is proposed. The proposed charger consists of two integrated stages. The 1st stage is Power factor correction (PFC) converter and the later one is the LLC resonant DC-DC converter. Both of these stages are driven by a common half-bridge network. The proposed charger is designed for charging a 100 cell 3.2kW Lithium-ion battery. The operation and performance of the proposed charger is evaluated by Spice based computer simulation. The simulation results showed that the proposed charger can efficiently charge the battery from depleted state to fully charged state.

Received date: 05-04-2023
Accepted date: 16-07-2023
Published date: 08-08-2023

Keywords: Battery charger, resonant converter, integrated battery charger, zero voltage switching, zero current switching

1. Introduction

A worldwide reality that has to be tackled with matters concerning environment, includes the polluted air which is caused by the gasses of fossil fuel utilized in transportation, exhaust gasses of industrial waste and power stations. So, the fossil fuels are being utilized to produce heat, electricity and transportation. The largest percentage of fossil fuel utilization is the gasoline and diesel-based transportations, which has increased the environmental pollution by burning of these harmful materials as the conventional vehicles uses the diesel engines. Therefore, the solution to these problems is the utilization of fossil safe energy means in which the electric vehicles is the best solution to reduce the fossil emission and the environmental pollution which caused by transportation [1].

Due to the benefits possessed by the Electric Vehicle in comparison to the fuel-engine based vehicle, the researchers are focusing on the development of electric vehicle battery chargers with the improved efficiency and best performance.

The battery charger basically consists of two stages in which 1st stage is the AC/DC converter stage with power factor correction and the 2nd stage is the DC-DC converter stage which regulates the output voltage and current according to requirement and type of the charger.

Referring to the standard SAE J1772 [27], there are two categories of battery charger. The on-board and the off-board battery charger. The on-board battery charger is preferred over the other type having the benefits of light weight, installation within the vehicle, cost effective and efficient operation. There are further two categories of the on-board type of battery charger, e.g. 1) two-stage battery charger and 2) single-stage/integrated two-stage battery charger. The two-stage battery charger comprises of the two types of converters e.g. 1st stage power factor correction converter and the 2nd stage DC-DC converter. These two stage converters are then combined to from a battery charging system. Conversely, the single stage battery charger performs the power factor correction and DC-DC converter operation in single-stage [27].

This paper focuses on the single-stage/integrated battery charger. Several works have been done on both type of battery chargers and there are different benefits and drawbacks of each topology. Some of them will be discussed in the next section.

A battery charger is an electronic circuit which is used to charge a depleted/rechargeable battery such as lithium-ion batteries or lithium polymer batteries. A battery consists of the cells which contains the charge and the battery is being utilized to provide the DC voltages to any electronic device. When it accomplishes its purpose then its cells need to be recharged.

The battery charger is the circuit which is designed to recharge the battery cells from depleted state to fully charged state.

As discussed in the previous section, * the single-stage battery charger consists of the integrated ac-dc power factor correction and the dc-dc resonant converter stage. The half bridge switches combine both the stages of the battery charger and performs the PFC operation and also gives the square wave input to the resonant converter. The resonant converter combined with the half bridge switches then performs the dc-dc operation [2]. The general structure of the single-stage battery charger is presented in figure 2.2 [3].

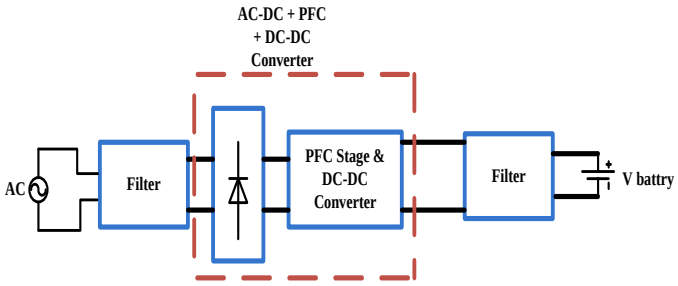

Figure 2. 2: General structure of Single-stage battery charger

The single-stage battery charger comprises of the integrated two-stages and as a result it can perform the battery charging operation with less switching devices in comparison to the conventional two-stage battery charger. The small number of switches in the single-stage battery charger reduces the conduction and switching losses so it increases the efficiency of the charging system. Moreover, the two-stage battery charger utilizes the DC link capacitor which increases the bulk and cost of the charger and decreases the efficiency, whereas the single-stage battery charger does not utilize the bulky dc link capacitor so it avoids the disadvantages produced by the capacitor. Furthermore, the two stage battery charger process the power in two stages and increase the losses whereas in the single stage battery charger the power is processed in the single stage and hence reduces the power losses with increased power conversion efficiency.

A single-stage battery charger with integrated two-stages is introduced in [47]. The battery charger consists of the bridge-less diodes circuit for ac-dc conversion and then the boost PFC and resonant dc-dc circuits share the same switches. The battery charger operates with continuous conduction mode and zero voltage switching of switching devices. The turn-off current variation of the charger is regulated. There are small number of electronic devices in the proposed circuit which reduces the conduction losses of the charging system. The circuit

operates for fixed input and fixed output application and generates the 48V output with 650W power. The schematic of the proposed charger is given in the figure 2.21.

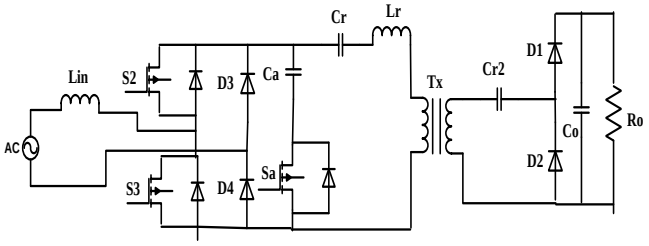

Figure 2. 1: Single-stage battery charger with integrated PFC and Resonant converter [47]

The single stage battery charger with novel ac-dc PFC and dc-dc converter is proposed in [48]. The proposed single-stage battery charger consists of the two bridge topologies which are connected in parallel with the ac source and in series with resonant tank. The two bridge topologies perform both, the ac-dc PFC operation and also operates as the input inverters for the dc-dc converter. The proposed converter is the bridge less topology as it removes the need of input bridge rectifier to perform the ac-dc conversion. It also eliminates the need of dc link electrolytic capacitor. Battery charger operates for 3kW fixed output power. The topology of the proposed converter is shown in figure 2.2.

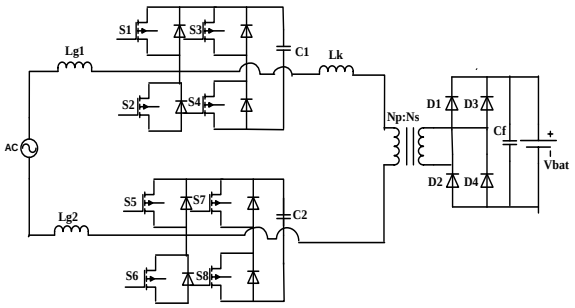

Figure 2. 2: Single-stage battery charger with two parallel connected bridge converters acting as the ac-dc converter with PFC and the input of dc-dc stage converter [48]

The topology presented in the previous work is the full-bridge converter at the input side and there is a linear transformer at the output side of the charger. There are different type of circuit techniques which are utilized for single-stage battery charger and each topology has its own advantages and drawbacks. A single-stage battery charger with full-bridge converter acting as the PFC stage and the input inverter of dc-dc stage with a center-tap transformer is presented in [49].

The circuit diagram is shown in figure 2.3.

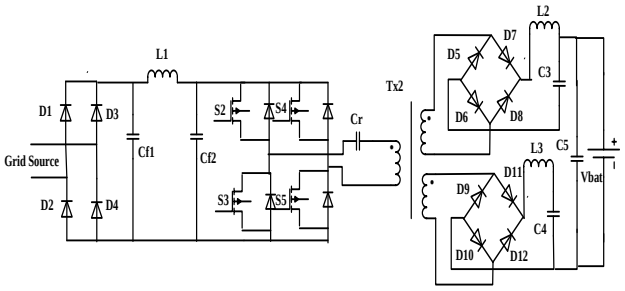

Figure 2. 3: Single-stage ac-dc converter for electric vehicle battery charger[49]

The proposed topology of single-stage battery charger operates efficiently for entire load range and gives the power factor correction operation for high and lower input voltage ranges. The charger is implemented for variable input and fixed output voltage and output power.

A single-stage battery charger comprises of the two integrated stages e.g. PFC and resonant dc-dc stage is discussed and implemented in [52]. The charger forms the resonant tank circuit by utilizing the leakage inductance of the transformer and the capacitor utilized to clamp the voltage of the 1st stage converter. The switch of the proposed topology operates with ZVS and ZCS which reduces the conduction losses along with the EMI filter size. The charger topology operates for the fixed output power of 3.2 kW. The circuit diagram is represented in the figure 2.4.

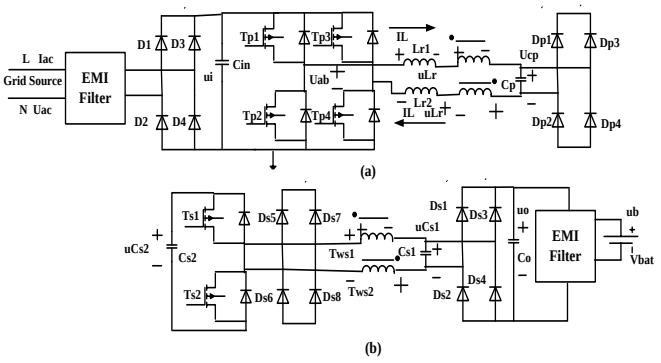

Figure 2. 4: Single-phase battery charger topology, consisting of two stage converters [52]

A single-stage LED driver circuit for the application of street-lightning is presented in [54]. The topology of the proposed system consists of the integrated two stages of the conventional battery charger, in which the half-bridge inverter combines the two boost circuits and the LLC resonant converter. The switches operates with ZVS which is not violated by the integration of two stages through the same half-bridge network. The LED driver is

implemented for the 100 W prototype which gives the maximum efficiency of 91% with power factor of 0.98. The topology of the system is presented in the figure 2.5.

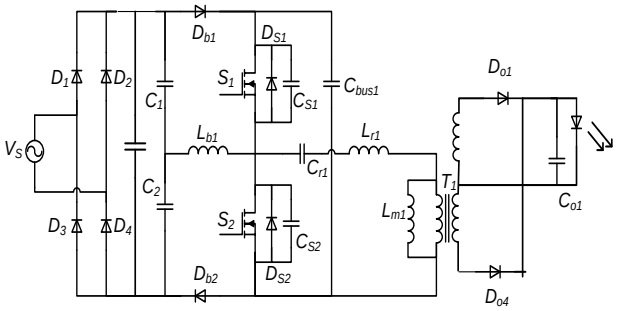

Figure 2. 5: Topology for the single-stage LED driver [54]

In this paper, the integrated single-stage EV battery charger topology has been presented which is the modified form of single-stage LED driver. The topology of the led driver has been implemented for single-stage battery charger which is itself a novelty in the previous work. Furthermore, the topology of the proposed battery charger is also modified with the requirement of application (single-stage battery charger) which is another novelty in the previous work.

2. Materials and Methods

3. Proposed single-stage Battery Charger

3.1 Circuit explanation

Figure presented in 3.1 presents the circuit topology of proposed single-stage electrical vehicle battery charger. It comprises of two power factor corrected isolated ac-dc converters which have parallel connection at the input side with ac source and series connection the output side with load. Each of the converters performs the Battery charging operation in two stages: 1st stage is the ac-dc with PFC converter along with dc-dc resonant converter stage. For example, the ac-dc stage of converter-1 consists of bridge rectifier (D1–D4), input inductor L1, capacitors C1 and C2 working as voltage divider, boost operation diodes Db1 and Db2, inductor Lb1 for boost operation, power processing switches S1 and S2, capacitor Cbus1 for bus voltage, while the dc-dc stage comprises of Cr1 as resonant capacitor, Lr1 as

resonant inductor and Lm1 as magnetizing inductor, T1 as power transformer, output bridge rectifier (Do1–Do4) and output capacitor Co1. The power mosfets S1 and S2 have the parasitic capacitors and diodes which are CS1 and CS2 and DS1 and DS2 respectively. The power switches S1 and S2 are common for both stages, therefore, these switches basically combine two stages and that's why the proposed converter is called single stage converter. Similarly, the ac-dc stage of converter-2 consists of bridge rectifier (D5–D8), input inductor L2, C3 and C4 as the voltage divider capacitors, Db3 and Db4 as the boost diodes, Lb2 as boost inductor, S3 and S4 power Mosfets, Cbus2 as the bus voltage capacitor while the dc-dc stage consists of resonant capacitor Cr2, the Lr2 as resonant inductor with Lm2 as magnetizing inductor, power transformer T2, output bridge rectifier (Do5–Do8) and output capacitor Co2. The power mosfets S3 and S4 have the parasitic capacitors and diodes which are CS3 and CS4 and DS3 and DS4 respectively. The power switches S3 and S4 are common for both stages, therefore, these switches basically combine two stages. The two stages are in parallel connection with a common input supply VS at the source side and they are connected in series with the load resistor RL at the output as given in Figure 3.1.

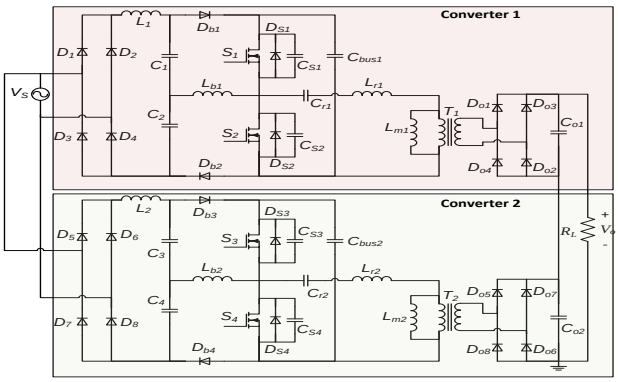

Figure 3. 1: Proposed single-stage electrical vehicle battery charger

The inductor L1 serves as filter inductor and the voltage divider capacitors have dual role in the circuitry i.e., they serve the purpose of input capacitor besides dividing the input voltage to half before supplying to the boost circuits. The input stage of each converter consists of two of boost circuits. For converter 1, the components Cbus1, Db1, Lb1, S1, with DS2 establish one boost topology, whereas components Cbus1, Db2, Lb1, S2, with DS1 establish the 2nd boost circuit. The bus capacitor Cbus1 and inductor Lb1 are commonly shared by both of the boost circuits of converter 1.

3.2 Principle of operation

The proposed electrical vehicle battery charger has two modes of operation namely independent mode and simultaneous mode. In independent mode only one of the two converters (let say converter 1) is operated at a time. This is done by blocking the gating signal to converter 2. Therefore, the output voltage of converter 2 is zero and only converter 1 produces output voltage. Consequently, the electrical vehicle battery charger's output voltage become half. Accordingly, this mode of operation can be used when electrical vehicle battery charger are requires the lower output voltages in deeply depleted state of the battery. In the simultaneous mode of operation both converters work together at a time and both converters produce output voltage. Therefore, the overall output voltage of the battery charger is addition of the output voltages of both converters. This mode of operation can be used when higher output voltages are required. So, this mode may be utilized to charge a moderately depleted battery. Therefore, proposed electrical vehicle battery charger can be implemented for charging an intensely depleted battery along with the moderately depleted battery.

The proposed electric vehicle battery charger operates in ten switching/operating cycles in which the last five modes are the replica of first five modes, so in this paper the first five modes will be presented.

Mode 1 (t0 − t1): Prior to the beginning of this mode power switch S2 was turned off and resonant current iLR1 started flowing through the output parasitic capacitors CS1 and CS2 of S1 and S2 respectively. As a result of which CS1 started discharging and CS2 started charging. This mode starts at time t0, at this time the parasitic capacitor CS1 which is connected to switch S1 was completely discharged, the voltage VDS1 of drain-source was reduced to zero and antiparallel DS1 diode of power switch S1 begins to conduct and CS2 was fully charged. The gate signal to switch S1 was applied to turn it on with ZVS. Simultaneously, the boost inductor Lb1 transfers its stored energy to Cbus1 through DS1, Db2, C1, and C2. The output diodes of secondary side Do1 and Do2 are turned with ZCS. Consequently, voltage across secondary winging of transformer T1 are clamped to Vo/2 and accordingly voltage across the primary winding are clamped to nV_o/2. Figure 3.3a represents the equivalent circuit of this mode of operation. The Cr1 as resonant capacitor and Lr1 as resonant inductor constitute a resonant tank circuit. The mode 1 terminates at time of t1 when resonant current ILr1 through resonant tank-1 reaches zero and output diode DS1 of switch S1 is turned OFF.

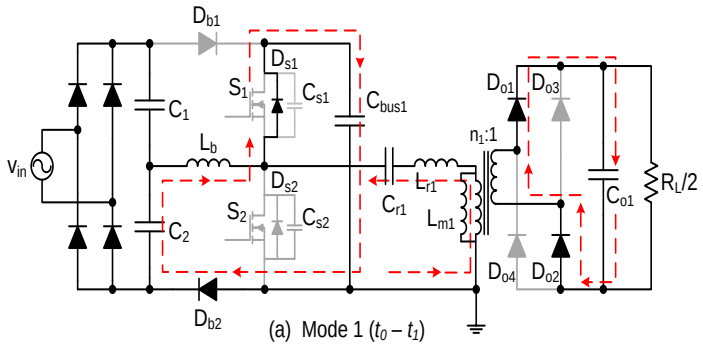

(a) Mode 1 ($t_0 - t_1$)

Mode 2 (t1 − t2): when the mode 2 starts, the resonant current ILr1 begins flowing in positive direction through power switch S1. The current rise in sinusoidal manner during this mode. The output diodes called as Do1 and Do2 are still conducting at the circuit's secondary side and output capacitor Co1 is charging. The mode is represented by the circuit diagram given in Figure 3.3b. At the last stage of mode two, The Lb1 boost inductor is fully discharged, current iLb1 approaches zero value and diode Db2 turns OFF.

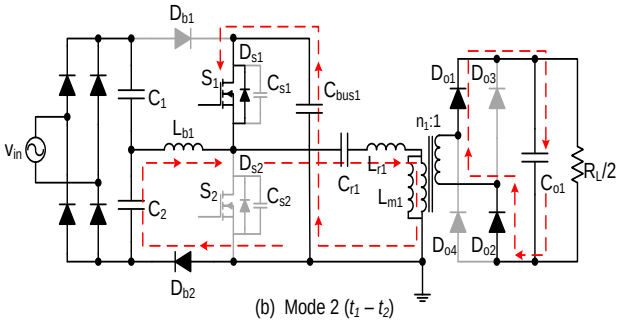

(b) Mode 2 ($t_1 - t_2$)

Mode 3 (t2 − t3): At the beginning of this mode, power switch S1 starts conducting and as a results C1 starts discharging and C2 starts charging via boost diode Db1. The current in boost inductor Lb1 is now increasing in the reverse direction. The current im1 of magnetizing inductor keep on rising linearly toward positive peak value and the resonant current iLr1 increases toward peak value and then decreases. The resonant current has higher value than magnetizing current and the difference current which is a half sinewave cycle propagates through the transformer's primary winding. The transformer secondary current which is also a half sinewave cycle flow through diodes Do1 and Do2 and charges output filter capacitor which supplies power towards the load. The mode 3 ends at the time when the resonant current becomes equal to magnetizing current and the primary/secondary current reduces to zero and output diodes Do1 & Do2 turns off with ZCS.

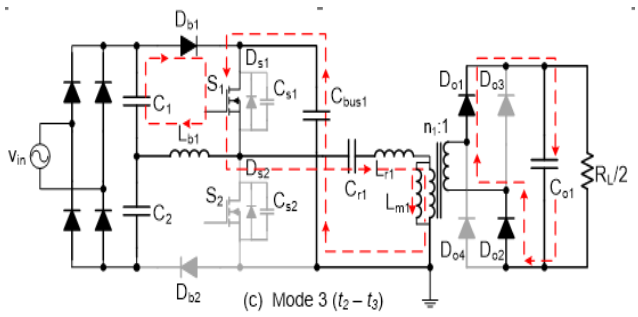

Mode 4 (t3 − t4): At the beginning of this mode, output diodes Do1 & Do2 were turned off with ZCS and hence filter capacitor starts supplying energy to load. As transformer primary and secondary current became zero at the beginning of this mode hence primary side circuit becomes independent from the secondary side circuit.

The voltage across magnetizing inductor are now no more clamped to Vo/2 and as a result inductor Lm1 started participating in resonance also with Lr1 and CR1. This mode ends when gate signal VGS1 of power switch S1 is removed.

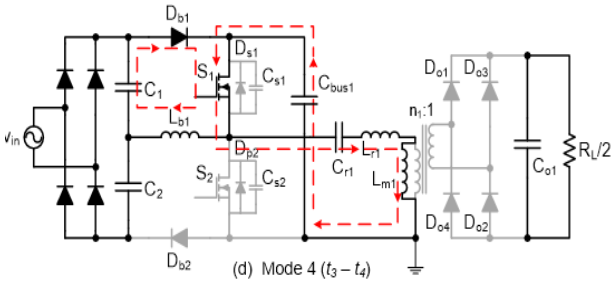

Mode 5 (t4 − t5): At time t4, power switch S1 was turned off with ZVS and it stopped conducting current. Therefore, its current diverted to parasitic capacitors CS1 and CS2. The parasitic capacitor CS1 which was initially having zero voltage across it started charging and CS2 which was initially fully charged up to bus capacitor voltage level started discharging. The power mosfet S1 along with CV charging modes is given in the Table 4.1.

Table 4. 1: Battery charging current, voltage, power and C-rate in CC and CV modes [37].

Key Point	Operating mode	V_{bat}	I_{bat}	P_o	Equivalent Resistance	C Rate
A	CC Mode	300	7.61A	2.28 kW	39. 42 Ω	1C
B		360	7.61A	2.74 kW	47.30 Ω	1C
C		420	7.61A	3.2 kW	55.19 Ω	1C
C	CV Mode	420	7.61–	3.2 kW	55.19 Ω	1C – 0.02C
D		420	0.152A	630W	2763 Ω	

turned off with ZVS because the charging process of parasitic capacitors CS1 reduces the rate of voltage rise across it and in the meantime, power switch completely turns off. At the termination of this mode capacitor CS1 is fully charged to bus capacitor's voltage level and CS2 is discharged to zero. Once the voltage VDS2 of drain-source is reduced to zero, the parasitic diode DS2 of power switch S2 is turned on and current begins flowing through it. The voltage across power mosfets S2 is clamed to zero and it can be turned on now with ZVS.

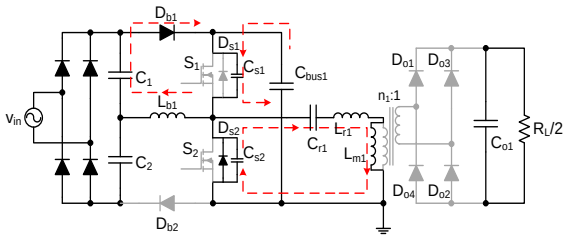

(e) Mode 5 ($t_4 - t_5$)

4. Design and Implementation

4.1 Design specifications for the proposed Electric Vehicle Battery Charger

The proposed battery charger is the single-phase ac to dc converter system that need to be designed for charging a 100 cell, 3.2 kW lithium-ion battery. The charging process of a normally depleted lithium-ion battery normally completes in two modes namely constant current and constant voltage modes. The charging current, voltage power and C-rate of battery in CC.

The input supply voltage to charger is 220Vrms at 50Hz. The output voltage of the charger ranges from 300V to 420V to charge the lithium-ion battery. Therefore, the design specifications for the proposed battery charger are given in Table 4.2.

Table 4. 2: Design parameters of proposed battery charger.

Parameters	Full-wave Bridge
Supply Voltage, v_{in}	220 V AC
Battery Capacity/rating	7.61 Ah / 3.2 kW
Input Frequency, f_{in}	50 Hz
Range of Output Power, P_o	63W – 3200W
Range of Output Voltage, V_o	300 V – 420 V
Output Current Range, I_o	0.152 A – 7.61 A
Load Resistor (range)	CC charging mode: 39.42 Ω – 55.19 Ω CV charging mode: 55.19 Ω – 2763 Ω
Expected efficiency, η	> 80%
Duty cycle, D	0.5

4.2 Design Procedure of Proposed EV Battery Charger

4.2.1 The Design procedure of the PFC circuit

The power factor correction circuit comprises two of boost circuits which are driven by half-bridge switching network operating with interleaved half switching cycle. The circuit consists of bridge rectifier, input inductor, voltage divider capacitors, boost inductor and boost diodes. The maximum voltage/current stress (rating) of these components is obtained in this section.

$$\boldsymbol{n_1 = M_1 \frac{V_{bus1}}{2V_{o1}} = M_2 \frac{V_{bus2}}{2V_{o2}}}$$

The input power of the charger is given by

$$\boldsymbol{P_{in} = V_S I_S cos\theta}$$

The maximum and minimum input current is given as:

$$\boldsymbol{i_{s(max)} = \frac{P_{in(max)}}{V_S} = \frac{P_{o(max)}}{\eta V_S}}$$

$$i_{s(min)} = \frac{P_{in(max)}}{V_S} = \frac{P_{o(min)}}{\eta V_S}$$

The size of input inductor is calculated from

$$L_{in} \cong \frac{(\Delta V_{C1}/2)}{2\Delta I_{Lin} f_S} = \frac{(\Delta V_{C2}/2)}{2\Delta I_{Lin} f_S}$$

The maximum current stress of the input inductor is equal to current stress on the bridge rectifier and it can be calculated from.

$$i_{Lin(max)} = \frac{P_{in(max)}}{V_S} = \frac{P_{o(max)}}{\eta V_S}$$

The voltage divider capacitors can be calculated from

$$C_1 = C_2 = \frac{\int I_{pk} dt}{V_p} = \frac{TI_{pk}}{2V_p}$$

4.2.2 Design procedure of the LLC Resonant DC-DC Converter

The corresponding equivalent ac load resistance Rac1 can be computed from

$$R_{ac1} = \frac{4{n_1}^2}{\pi^2} R_o$$

The maximum and minimum value of voltage gain of each converter is

$$M_{min} = \frac{2n_1 V_{o,min}}{V_{bus,max}} \cong 1.0$$

$$M_{max} = \frac{2n_1 V_{o,max}}{V_{bus,min}} = 2.1$$

The resonant capacitor's minimum value can be calculated as

$$C_{r,min} = \frac{P_o}{4n_1 V_o f_{s,min}(V_{bus,max} - nV_o)}$$

The voltage stress on resonant capacitor is calculated from

$$V_{cr,max} = n_1 V_{o1} + \frac{P_o}{4 n_1 V_{o1} f_{s,min} C_{r1}}$$

The value of resonant inductor may be obtained by substituting these values in (4.9).

$$L_{r1} = C_{r1}(Q_1 R_{ac1})^2$$

The value of magnetizing inductor can be calculated as.

$$L_{m1} = k_1 L_{r1}$$

The 1st and 2nd resonant frequencies of the converter can now be determined from (4.11) and (4.12) as follows.

$$f_{r1} = \frac{1}{2\pi\sqrt{C_{r1} L_{r1}}}$$

$$f_{m1} = \frac{1}{2\pi\sqrt{C_{r1}(L_{r1} + L_{m1})}}$$

4.3 PSpice simulation of the Overall System

The maximum value of voltage and current stresses on the circuit components which was calculate in the previous sections are summarized in Table 4.3.

Table 4. 3: The maximum value of voltage and current stresses on the circuit components

Component	Symbol	Voltage Stress	Current Stress
Input full-bridge rectifier		$v_{s(max)}$	$i_{s(max)}$
Voltage divider capacitors	C_1, C_2, C_3, C_4	$\frac{v_{s(max)}}{2}$	$\frac{i_{s(max)}}{2}$
Boost diodes	D_1, D_2, D_3, D_4	V_{bus1}	$i_{s(max)}$
Boost inductor	L_{b1}, L_{b2}	V_{bus1}	$i_{s(max)}$
Power switches	S_1, S_2, S_3, S_4	V_{bus1}	-
Bus voltage capacitor	C_{bus1}, C_{bus2}	V_{bus1}	-
Resonant capacitor	C_{r1}, C_{r2}	$V_{cr,max}$	I_r
Output diodes	$D_{o1} - D_{o8}$	V_o	I_o

The proposed circuit was implemented in PSpice software using component values calculated in previous sections. The schematic of power topology which was implemented in PSpice is presented by the Figure 4.2.

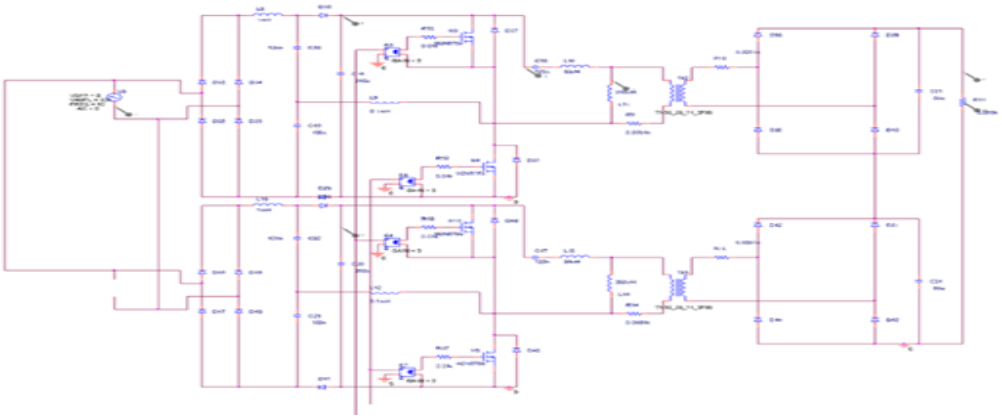

Figure 4. 2: The PSpice schematic circuit diagram of power topology of proposed charger.

3. Results

The proposed EV battery charger was simulated in PSpice software to evaluate its performance at three key points namely point A, point B and point C. The results obtained are presented in following section.

5.1 Result at Key Point A (Vbat = 300V, Ibat=7.61A and Po= 2.2kW)

First of all, charger was simulated at point A and results obtained are presented in Figures 5.1 – 5.10. This point is basically the starting point of CC charging mode. The simulated results for the output voltage as Vo with the output current as Io are represented in the Figure 5.1. The output voltage is approximately 300 V and output current is 7.61 A. The charger has the output power of approximately 2.2 kW. The ripple voltage in the output of battery charger is 10 V approximately, thus, the ripple percentage of the output voltage is 3.33%.

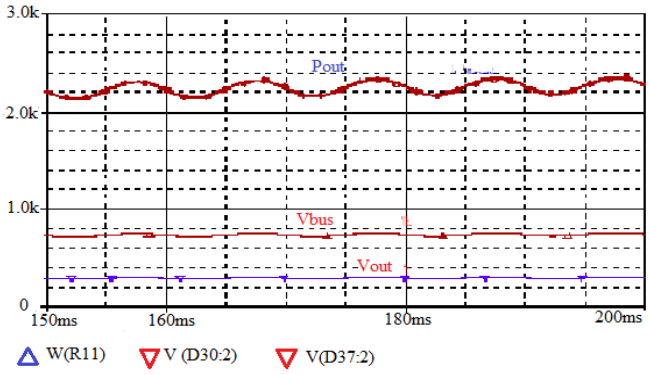

Figure 5. 1: Simulated results of output voltage as Vo with the output current as Io at 2.2kW.

Figure 5.2 presents the output voltage along with the current of the battery charger for output power of 2.2 kW at the start-up process. The output voltage of the battery charger reaches steady state within 140 ms approximately.

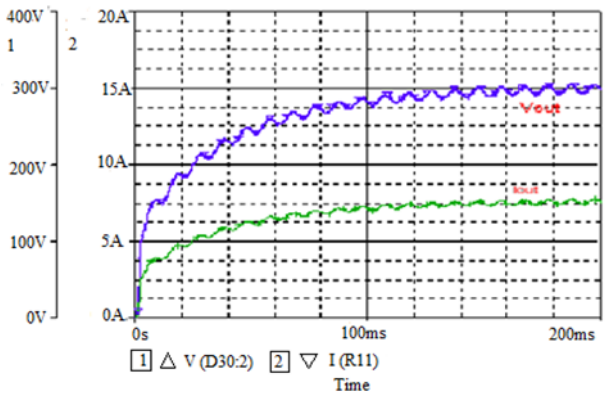

Figure 5. 2: Simulated waveforms of output voltage and current during start-up.

In Figure 5.3, the simulated waveforms of voltages and currents of diodes Do1 and Do2 of the output bridge rectifier of battery charger are depicted. It can be seen from the figure that the voltage across diodes are zero for turning-on and turning-off time of the diodes. Therefore, the diodes of the output bridge rectifiers are operating with ZCS and accordingly their switching power loss is negligible. The peak voltage across the diodes are 150V and peak current is 15A in this case.

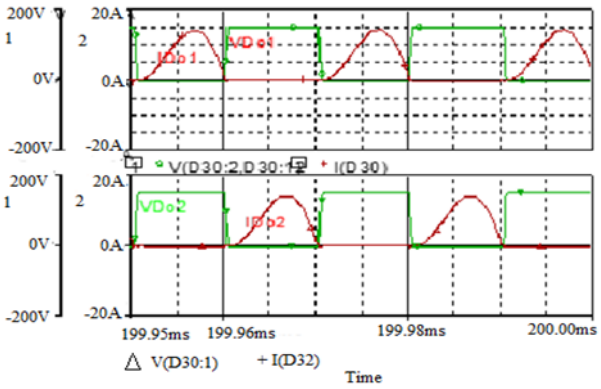

Figure 5. 3: Simulated waveforms of diode voltage VDo1, VDo2 and current IDo1, IDo2.

Figure 5.4 presents the simulated results for the drain-source voltage as VDS1, the iLr known as resonant current, the secondary side voltage Vsec-1 with secondary side current isec-1 for output 2.2 kW output power. The operating frequency of the converter for this operating point is 50kHz, i.e. equal to its resonant frequency. The peak value of resonant and magnetizing currents is 10A and 8A respectively and peak value of tank voltage is 800V. On the secondary side, the peak value of voltage is 150V and peak secondary current is 15 A. The voltage and current stress on the output diodes is 150V and 15 A respectively.

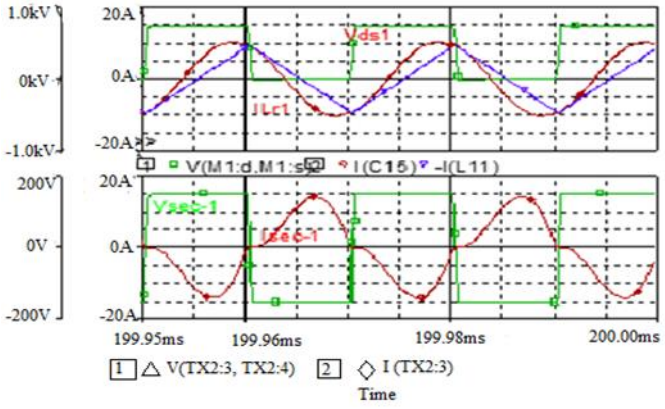

Figure 5. 4: PSpice simulated waveforms for the drain-source voltage VDS1, the resonant current iLr, the secondary side voltage Vsec-1 and secondary side current isec-1 at 2.2 kW output power.

Figure 5.5 gives the simulated waveforms for the drain and source voltages as VDS1 with VDS2 , the voltages between gate and source as VGS1 and VGS2 of the switches S1 with S2 respectively. It can be seen from the figure that drain-source voltages of both the switches approaches to zero before the rise of their gate signals. This means both switches turn on

under zero voltage conditions. Moreover, it also can be seen from the figure gate-source signal's voltage level reduced to zero before the rise of drain-source voltages of the switches. This mean both switches realize zero voltage switching turn off. Hence their switching power loss is negligible. The amplitude of drain-source voltage is 800 V, therefore the voltage stress on switches in this mode is 800V.

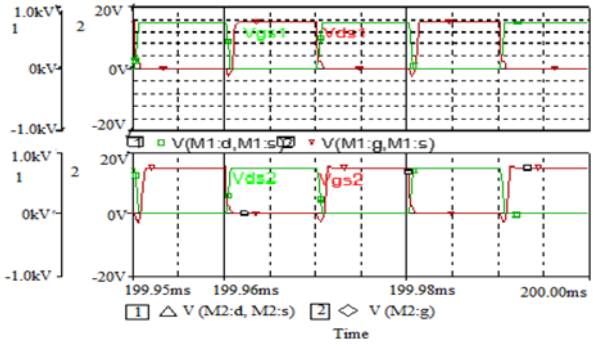

Figure 5. 1: PSpice simulation results of the drain to source voltages as V_{DS1}, with V_{DS2}, the voltages between gate and source as V_{GS1} and V_{GS2} of the power mosfets S_1 with S_2 respectively.

Figure 5.6 shows the simulated waveforms of output voltage of input bridge rectifier of converter 1 and high frequency current of boost inductor Lb1. This current consists of high frequency pulses and their frequency is equal to switching frequency of the converter. These pulses are making envelopes at the twice of input frequency. The inducor gives the maximum current value of 32A in this case. Figure 5.7 shows the simulated waveforms of input rectified voltage and input rectified current flowing through input inductor of converter 1. The rectified voltage is in-phase with the rectified current and their frequency is twice the frequency of input voltage and current. It can be seen that the distortion in the input rectified current is negligible. The peak value of input rectified current is 9A approximately.

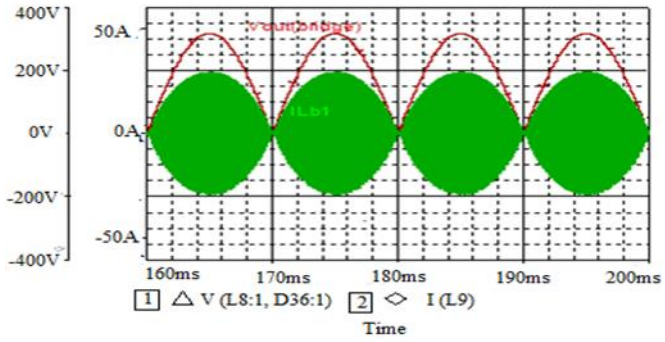

Figure 5. 6: Simulation results of boost inductor's current, iLb.

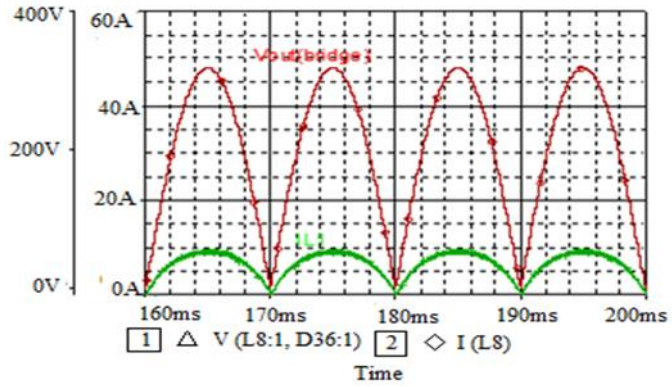

Figure 5.7: Simulation results of output voltage of input bridge rectifier and current of input inductor L1.

Figure 5.8 shows the simulated waveforms of input voltage VS and input current IS. The peak value of input current is 18 A approximately. This is because the overall input current is sum of input currents of two converters. It can be seen from the figure that the phase shift between input voltage and current is zero. The input power factor can be computed from following equation.

$$PF = \frac{I_{1,rms}}{I_{rms}} cos\,\theta_1$$

where Irms with the I1rms are the rms parameters of source current and fundamental component of the input current with the input voltage, respectively, the phase-angle between the fundamental components of input voltage and current is θ1.

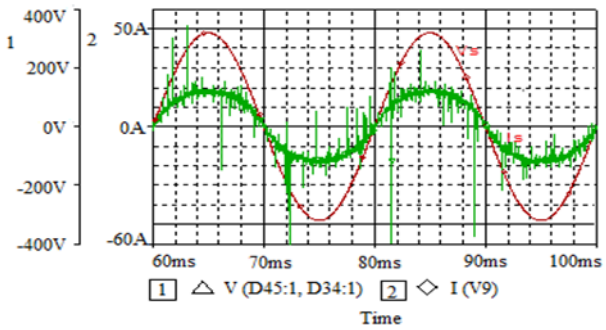

Figure 5.8: PSpice simulation results of source voltage as vin and the source current iin

5.2 Results at Key Point B (Vbat = 420V, Ibat=7.61A and Po= 3.2kW)

Next to evaluate the operation of charger at peak power point, the converter was operated at point B, i.e. at Vbat = 420V, Ibat=7.61A and Po= 3.2kW. This point is basically the termination point for the CC mode of charging also the starting point for CV charging mode. The results obtained are presented in Figures 5.9 – 5.17. The simulated waveforms for output voltage called as Vo with the output current as Io is represented in Figure 5.9. The voltage at the output is approximately 418.5 V with output current of 7.61 A.

The output power of charger is approximately 3.2 kW. The ripple voltage in the output of battery charger is 1.5 V approximately, therefore, the percent output voltage ripple is 0.35%. Figure 5.10 gives output voltage with the current of the battery charger for output power of 3.2 kW for the duration of start-up process. The output voltage of the battery charger reaches steady state within 70 mS approximately.

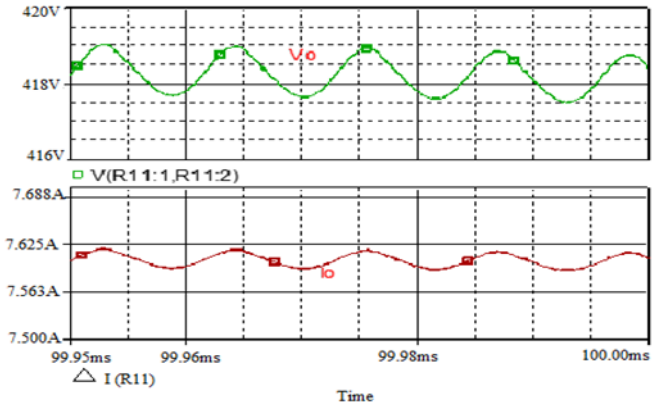

Figure 5.9: Simulated results of Vo output voltage along with the current Io at 3.2kW.

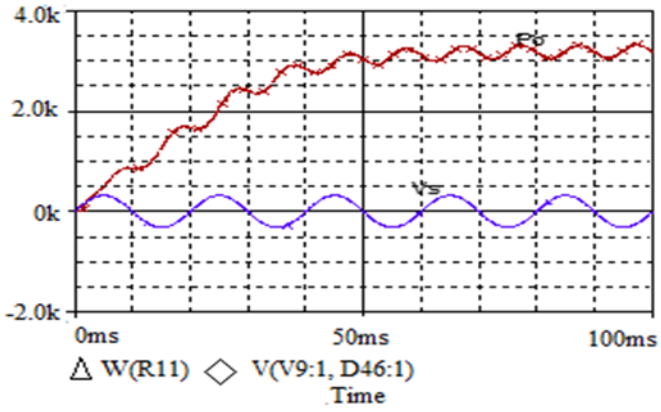

Figure 5.10: Simulated waveforms of output Power and input voltage during start-up.

In Figure 5.11, the simulated waveforms of voltages and currents of diodes Do1 and Do2 of the output bridge rectifier of battery charger are depicted. It can be seen from the figure that the voltage across diodes are zero for the turning-on and turning-off time of the diodes. Therefore, the diodes of the output bridge rectifiers are operating with ZCS and accordingly their switching power loss is negligible. The peak voltage across diodes in this case are 2.10V and maximum current flowing through diodes is 17A.

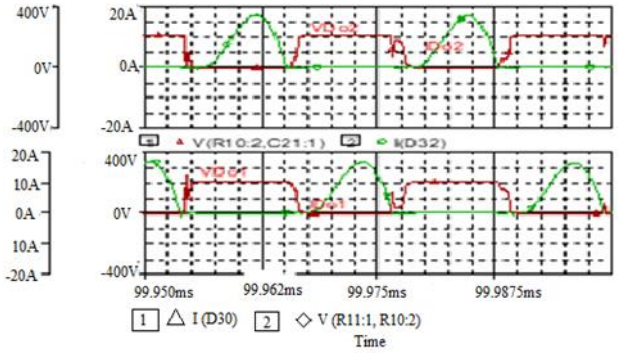

Figure 5.11: Simulated waveforms for diode voltage VDo1, VDo2 with current IDo1, IDo2.

Figure 5.12 shows the simulated waveforms for the drain to source voltage as VDS1, the resonant current iLr, the secondary side voltage Vsec-1 and secondary side current isec-1 for output 3.2 kW output power. The maximum voltages across power switches are 900V and current is 13A. The peak value of resonant and magnetizing inductor current is approximately equal. The peak value of secondary voltage 2.10V and peak secondary current is 17A.

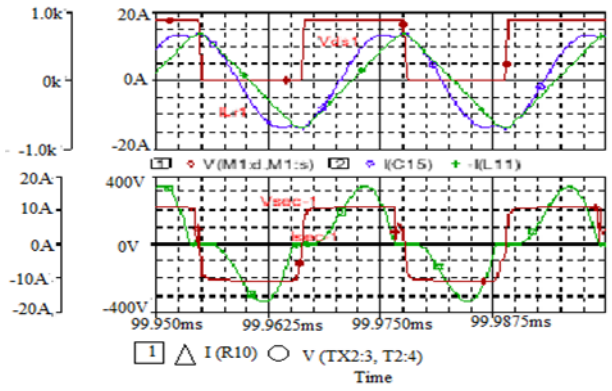

Figure 5.12: Simulated waveforms for the drain and source voltage as VDS1, resonant current iLr, the secondary side voltage Vsec-1 and the secondary side current isec-1 at 3.2 kW output power.

Figure 5.13 presents the simulated waveforms for the drain and source voltages VDS1, with VDS2, the voltages between gate and source VGS1 and VGS2 of the power mosfets S1 with S2 respectively. It can be seen from the figure that the drain-source voltages of both switches reduce to zero before the rise of their gate signals even in this case. This means both switches turn on under zero voltage conditions. Moreover, it also can be seen from the figure gate-source signal's voltage level reduced to zero before the rise of drain-source voltages of the switches. This mean both switches realize zero voltage switching turn off. Hence their switching power loss is negligible. The amplitude of drain-source voltage is 900 V, therefore the voltage stress on switches in this mode is 900V.

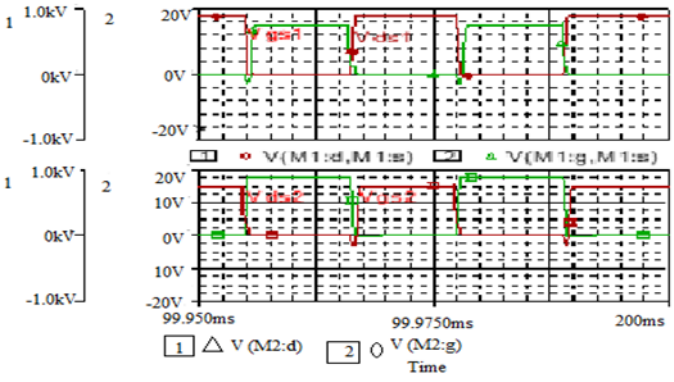

Figure 5.13: Simulation waveforms for the drain and source voltage as VDS1, with VDS2, the voltage between gate and source VGS1 and VGS2 of the power mosfets S1 with S2 respectively.

Figure 5.14 shows the simulated waveforms of high frequency current of boost inductor Lb1. This current consists of high frequency pulses and their frequency is equal to switching

frequency of the converter. These pulses are making envelopes at twice the input frequency. The highest value of current through inductor in this case is 64A.

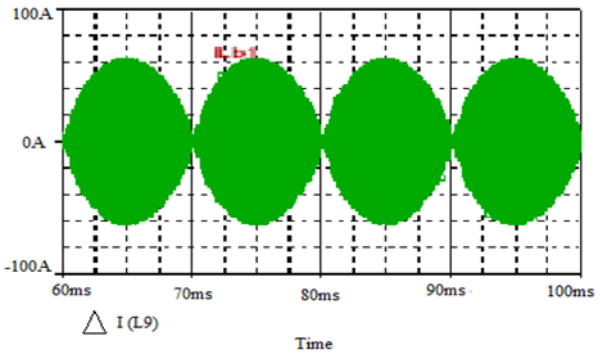

Figure 5.14: Simulation results of current, iLb of the boost inductor.

Figure 5.15 shows the zoomed view of simulated waveforms of boost inductor's current, iLb1 and gate signal of S2.

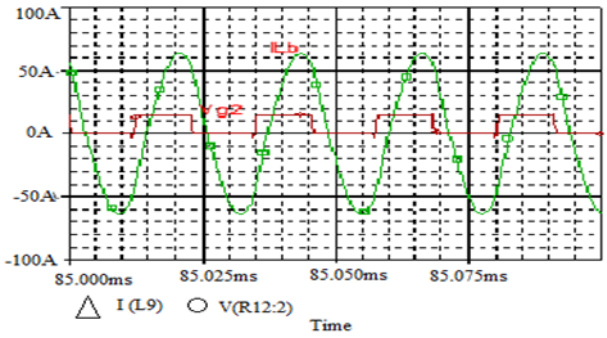

Figure 5.15: Zoomed view of simulated waveforms of boost inductor's current, iLb1 and gate signal of S2.

Figure 5.16 gives the simulated results of output voltage with the output current of input bridge rectifier of converter 1. The rectified voltage is in-phase with the rectified current and their frequency is twice the frequency of input voltage and current. It can be seen that the distortion in the input rectified current is negligible. The peak value of input rectified current is 19A approximately.

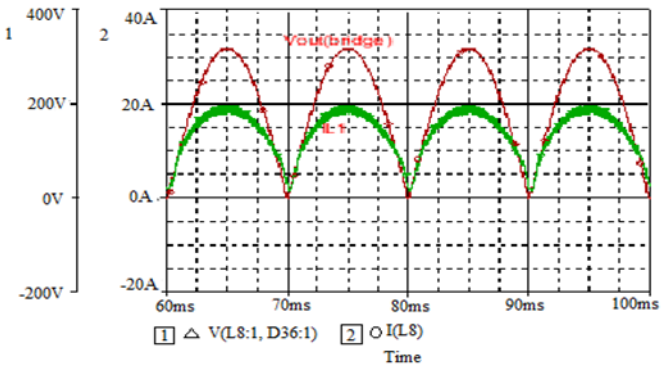

Figure 5.16: Simulation results of output voltage of input bridge rectifier and current of input inductor L1.

Figure 5.17 shows the simulated waveforms of input voltage VS and input current IS. The peak value of input current is 35 A approximately. This is because the overall input current is sum of input currents of two converters. Moreover, the input current is in phase with input voltage and shape of input current is nearly sinusoidal. Therefore, input power factor is above 0.9-

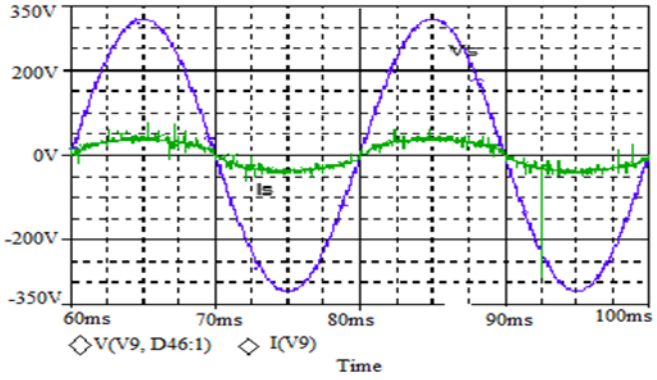

Figure 5.17: Simulation results of the source voltage vin and the source current iin

5.3 Results at Key point C (Vbat = 420V, Ibat=0.152A and Po= 0.63kW)

Next to evaluate the operation of charger at end point, the converter is operated at the point C, i.e. at Vbat = 420V, Ibat=0.152A and Po= 0.63kW. This point is the end point of the CV charging mode i.e. battery charging completes at this point. The results obtained are presented in Figures 5.18 – 5.25. The simulated results of output voltage as Vo and the output current as Io is represented in the Figure 5.18. The output voltage is approximately 420 V and output current is 0.152 A.

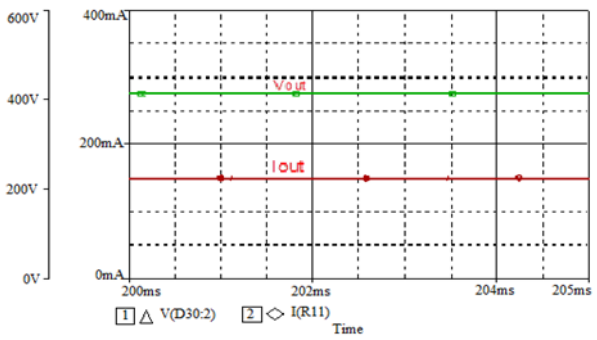

Figure 5.18: Simulated waveforms for the output voltage as Vo with current Io for 0.63kW.

The output power of charger is approximately 0.63 kW. The ripple voltage in the output of battery charger is negligible in this case as load is very light.

In Figure 5.19, the simulated waveforms of voltages and currents of diodes Do1 and

Do2 of the output bridge rectifier of battery charger are depicted. It can be seen from the figure that the voltage across diodes are zero for the turning-on and turning-off point of the diodes. Therefore, the diodes of the output bridge rectifiers are operating with ZCS and accordingly their switching power loss is negligible. The maximum value of voltage across diodes in this case are 210V and maximum current flowing through diodes is 0.6A.

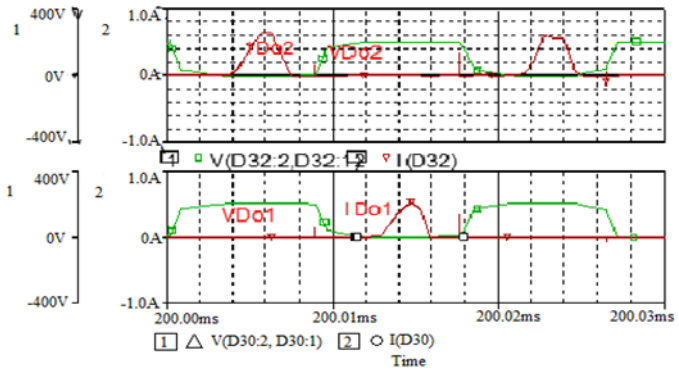

Figure 5.19: Simulated waveforms of diode voltage VDo1, VDo2 and current IDo1, IDo2.

Figure 5.20 gives the simulated results of drain and source voltage as VDS1, the iLr resonant current, the secondary side voltage Vsec-1 with secondary side current isec-1 for output 0.63 kW output power. The maximum voltages across power switches are 1100V and current is 10A. The peak value of resonant and magnetizing inductor current is approximately equal. The peak value of secondary voltage 210V and peak secondary current is 0.6A.

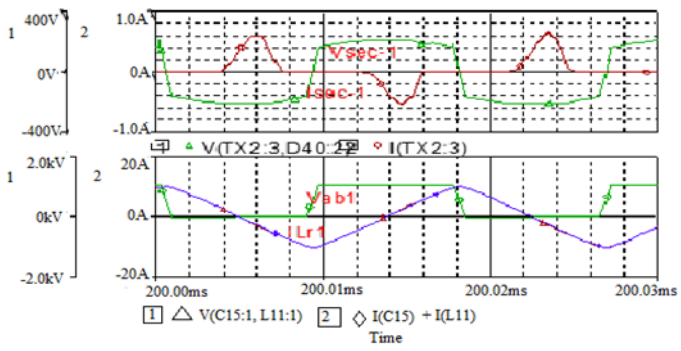

Figure 5.20: Simulated waveforms for the drain and source voltage as VDS1, the iLr resonant current, the secondary side voltage Vsec-1 with the secondary side current isec-1 at 0.63 kW output power.

Figure 5.21 displays the simulated waveforms for the drain and source voltage as VDS1, with VDS2 and voltages between gate and source VGS1 with VGS2 of the power mosfets S1 along with S2 respectively. It can be seen from the figure that the drain-source voltages of both switches reduce to zero before the rise of their gate signals even in this case. This means both switches turn on under zero voltage conditions. Moreover, it also can be seen from the figure gate-source signal's voltage level reduced to zero before the rise of drain-source voltages of the switches. This mean both switches realize zero voltage switching turn off. Hence their switching power loss is negligible. The amplitude of drain-source voltage is 1100 V, therefore the voltage stress on switches in this mode is 1100V.

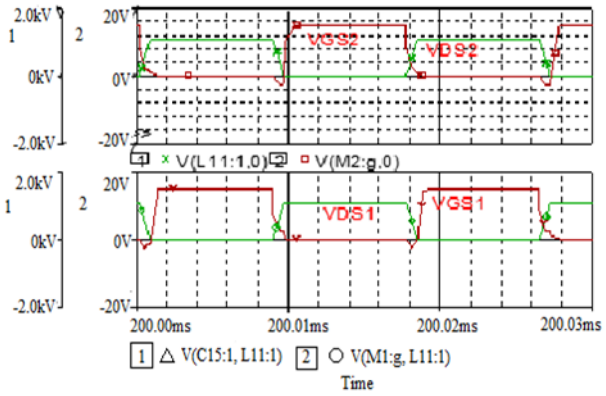

Figure 5.21: Simulation waveforms for the drain-source VDS1 voltage, VDS2 with the gate to source VGS1 voltage and VGS2 of the power mosfets S1 with S2 respectively.

Figure 5.22 shows the simulated results of high frequency current of boost inductor Lb1. This current consists of high frequency pulses and their frequency is equal to switching frequency

of the converter. These pulses are making envelopes at the twice of input frequency. The inductor gives the maximum current value of 20A in this case.

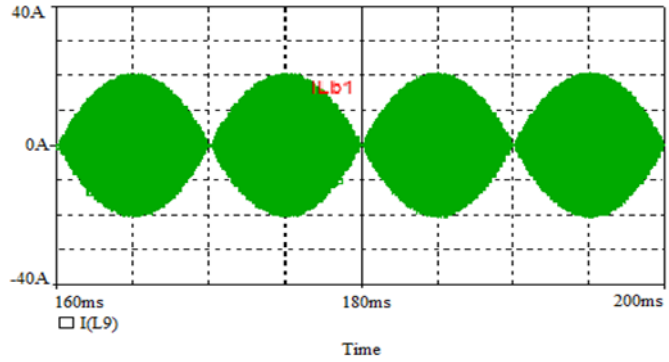

Figure 5.22: Simulation results for current, iLb of the boost inductor.

Figure 5.23 shows the zoomed view of simulated waveforms of boost inductor's current, iLb1 and gate signal of S2.

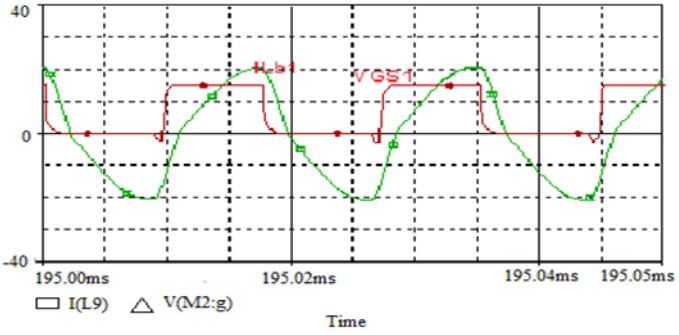

Figure 5.23: Zoomed view of simulated waveforms of boost inductor's current, iLb1 and gate signal of S2.

Figure 5.24 explains the simulated results for output voltage with the output current of input bridge rectifier of converter 1. The rectified voltage is in phase with the rectified current and their frequency is twice the frequency of input voltage and current. It can be seen that the distortion in the input rectified current is negligible. The peak value of input rectified current is 06A approximately.

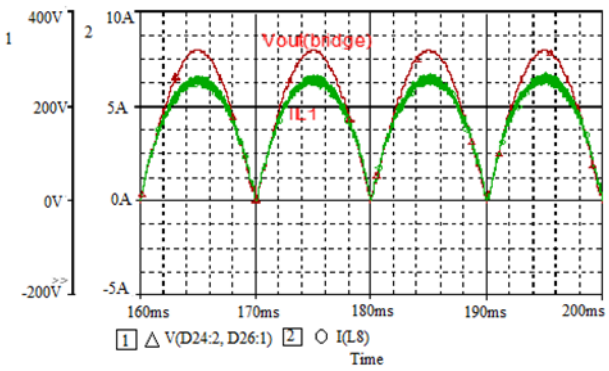

Figure 5.24: Simulation results of output voltage of input bridge rectifier and current of input inductor L1.

Figure 5.25 gives the simulated waveforms of input voltage VS and input current IS. The peak value of input current is 12 A approximately. This is because the overall input current is sum of input currents of two converters. Moreover, the input current and voltage are in phase with each other and shape of the input current becomes nearly sinusoidal. Therefore, input power factor is above 0.95.

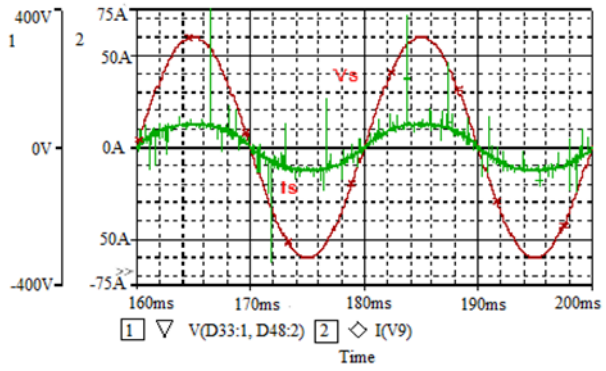

Figure 5.25: Simulation results of input voltage as vin with the input current as iin.

4. Conclusions

The transportation in the highly populated Urban areas is going to be preferred by using the Electric vehicle as a conveyance. With the demand of electric vehicle to be utilized for transportation, the use and development of battery chargers will also increase in a large amount. There are many topologies which have been discussed in the literature and each has its own advantages and drawbacks as well and focus of research is on the development of

efficient battery chargers with wide output voltage range that can handle the battery voltages in deeply depleted and also the normally depleted state.

In this research project, the single-stage on board battery charger for plugged-in electric vehicles is proposed, designed and simulated for analysis of results and performance evaluation. The implemented battery charger performs the AC-DC conversion with the power factor correction of input voltage and current and then the LLC Resonant DC-DC converter performs the output voltage regulation. The battery charger consists of the two converters in parallel connection at the input side and in series connection on the output side. These two converters can operate independently and simultaneously to charge the normally depleted and the deeply depleted battery respectively. The simulation results are presented for three operating points showing the wide output voltage and power range e.g. the minimum output power 0.63kW at V_bat=420V, the medium output power 2.2kW at V_bat=300V and the maximum output voltage 3.4kW at V_bat=420V. The charger operates for greater than 80% efficiency with 0.99 power factor. The charger also achieves the ZVS and ZCS operation for primary and secondary side switches so the switching losses are negligible improving the efficiency of the charger. Furthermore, The battery charger topology can be modified as the single –stage integrated charger with the 5 element resonant tank converter for the 2nd stage of charger, to simulate for more efficient results.

The battery charger switching operation can controlled by using additional resonant current control circuitry/ control algorithm which will automatically adjusts the switching frequency of mosfets according to the terminal voltage of the depleted battery. The battery charger topology can be modified further to operate for wider output voltage range, by increasing the number of cascaded converters.

References

1. L. Jie, "Environmental Effects of Vehicle Exhausts, Global and Local Effects – A Comparison between Gasoline and Diesel," Halmstad University, Halmstad , 2011.

2. "SAE Electric Vehicle and Plug-in Hybrid Electric Vehicle Conductive," SAE Std. J1772, 2010.

3. A Novel Economical Single Stage Battery Charger with Power Factor Correction (01179300) Alisha

4. A Multi-Device Front-end Power Factor Converter for EV Battery Charger (7) Ms Thesis

5. M. Alam, W. Eberle and F. Musavi, A Single-Stage Bridgeless High Efficiency ZVS Hybrid-Resonant Off-Road and Neighborhood EV Battery Charger, IEEE, 2014.
6. B. Kim, M. Kim and S. Choi, "Single-stage Electrolytic Capacitor-less AC-DC Converter with High frequency isolation for EV Charger," in proc. IEEE Power Electronics and Motion Control Conf., (IPEMC-ECCE Asia), 2016.
7. S. Hattori and F. Kurokawa, "Single Stage AD-DC Full-bridge Converter for Battery Charger," in Proc. IEEE Inter. Telecom. Conf., Oct. 2015.
8. S. Li, J. Deng and C. Chris, "Single-Stage Resonant Battery Charger With Inherent Power Factor Correction for Electric Vehicles," IEEE Trans. on Veh. technol., vol. 62, no. 9, pp. 4336-4344, Nov. 2013.
9. Y. Wang, Y. Guan, K. Ren, W. Wang and D. Xu, "A Single-stage LED Driver Based on BCM Boost Circuits and LLC Converter for Street Lighting system," IEEE Trans.on Ind. Electron., vol. 62, pp. 5446-5457, 2015.
10. H. Wang and A. Khaligh, "Comprehensive Topological Analyses of Isolated Resonant Converters in PEV Battery Charging Applications," in proc. IEEE Transpor. Electrification Conf., June 2013.